A NEW "FREE-FLIGHT" MOUNT SYSTEM FOR HIGH-SPEED WIND-TUNNEL FLUTTER MODELS

Wilmer H. Reed III and Frank T. Abbott, Jr.

NASA Langley Research Center
Langley Station, Hampton, Va.

Presented at the Symposium on Aeroelastic and Dynamic Modeling Technology

Dayton, Ohio,
September 23-25, 1963

A NEW "FREE-FLIGHT" MOUNT SYSTEM FOR HIGH-SPEED WIND-TUNNEL FLUTTER MODELS

By Wilmer H. Reed III and Frank T. Abbott, Jr.

NASA Langley Research Center

ABSTRACT

15636

Wind-tunnel investigations of aeroelastic models often require that rigid body as well as elastic modes of the test article be simulated. In effect, the mount system must allow the model to be "flown" in the test section and have negligible aerodynamic interference at transonic Mach numbers. Such a system has been developed for flutter and gust response investigations on complete models in the NASA Langley transonic dynamics tunnel. The system consists of a pair of cables which pass through pulleys in the model and run upstream and downstream of the test section in mutually perpendicular planes. Stability and natural frequencies of the cable-supported model are controlled by the preload tension in a spring in one of the cables. The paper describes some evaluation tests and presents a stability analysis which shows the influence of various parameters that govern dynamic characteristics of the system.

A NEW "FREE-FLIGHT" MOUNT SYSTEM FOR HIGH-SPEED WIND-TUNNEL FLUTTER MODELS*

By Wilmer H. Reed III and Frank T. Abbott, Jr.

NASA Langley Research Center

INTRODUCTION

Wind-tunnel investigations in such areas as flutter, gust response, dynamic stability and the like often require that the dynamic behavior of the test article in free flight be simulated. For example, flutter instabilities on an aircraft may involve interaction between elastic and rigid-body modes. If, in wind-tunnel studies of the problem, these modes are significantly altered by constraining forces associated with the model support device, corresponding alterations in the flutter characteristics of the model as compared with those of the free-flying aircraft might be expected. On the other hand, if the model is mounted in some arbitrary manner that might permit simulation of free-flight rigid-body modes, we have no guarantee that the resulting system will be satisfactory. In fact, without careful consideration of the dynamics of the overall system, violent instabilities may occur, making the dynamic behavior of the model on its mount strikingly different from what it would be in free flight.

The present paper concerns a new free-flight mount system that has been developed for flutter and gust response studies in the NASA Langley transonic dynamics tunnel. Practical experience with the present and some earlier mount systems is described, and a stability analysis presented to show the influence of various controllable parameters in the dynamic characteristics of the system.

SYMBOLS

a	horizontal distance between center of gravity and outer cable-tangency-point on rear pulleys (positive when c.g. ahead of rear pulleys)
b	span of wing
c	mean aerodynamic chord

*Patent disclosure submitted.

a_{ij}, b_{ij}, c_{ij} coefficients in longitudinal equations of motion

$\bar{a}_{ij}, \bar{b}_{ij}, \bar{c}_{ij}$ coefficients in lateral equations of motion

d horizontal distance between model plane of symmetry and outer cable-tangency-point on rear pulleys

e horizontal distance between model center of gravity and outer cable-tangency-point on front pulleys

g acceleration due to gravity

h vertical distance between model center of gravity and outer cable-tangency-point on front pulleys

I_{xz} product of inertia

k spring constant

k_{ij} cable stiffness influence coefficient giving increment in cable restraining forces or moments in mode i due to unit deflection in mode j

l_i length of cable i from wall attachment point outer cable-tangency-point on pulley i

L, M, N roll, pitch, and yaw moments about x-, y-, and z-axes, respectively

m mass of model including pulleys

N_{SF} static stick-fixed-neutral point

q dynamic pressure, $\frac{1}{2}\rho U^2$

r_x, r_y, r_z radius of gyration about x-, y-, and z-axes, respectively

s Laplace operator

S wing area

U wind-tunnel test-section velocity

W weight of model including pulleys

x, y, z displacement coordinates of model center of gravity

X, Y, Z external forces on model

C_D coefficient of drag, $\frac{\text{Drag}}{qS}$

C_{D_o} C_D at $\alpha = 0$

C_L coefficient of lift, $\frac{\text{Lift}}{qS}$

C_{L_o} C_L at $\alpha = 0$

C_l rolling-moment coefficient, $\frac{\text{Rolling moment}}{qSb}$

C_m pitching-moment coefficient, $\frac{\text{Pitching moment}}{qSc}$

C_{m_o} C_m at $\alpha = \delta = 0$

C_n yawing-moment coefficient, $\frac{\text{Yawing moment}}{qSb}$

C_y side-force coefficient, $\frac{\text{Side force}}{qSc}$

α angle of attack, $\theta_o + \theta + \frac{\dot{z}}{U}$

β angle of sideslip, $\frac{\dot{y}}{U} - \psi$

β_1, β_2 angle in vertical plane between x axis and cables 1 and 2, respectively

β_3, β_4 angle in horizontal plane between x axis and cables 3 and 4, respectively

β_R angle in horizontal plane between x axis and rear cables for trimmed flight

δ_o elevator deflection angle for trimmed flight

ζ_i effective viscous damping ratio of mount in mode i for no wind condition

$\bar{\zeta}$ damping ratio of model in flight

η real part of root of characteristic equation

θ pitch angle pertubation from trim condition

θ_o pitch angle of trimmed flight

$\bar{\theta} = \theta_o + \theta$

ρ mass density of wind-tunnel test medium

$\sigma = \frac{\rho US}{2m}$

φ angle of roll

ψ angle of yaw

ω circular frequency

$\omega_{ij} = \sqrt{\frac{k_{ij}}{m}}$

ω_n undamped natural frequency

Stability derivatives are indicated by subscript notation; for example:

$$C_{l_r} = \frac{\partial C_l}{\partial\left(\frac{\dot{\psi}b}{2U}\right)} \qquad C_{n_p} = \frac{\partial C_n}{\partial\left(\frac{\dot{\varphi}b}{2U}\right)} \qquad C_{m_q} = \frac{\partial C_m}{\partial\left(\frac{\dot{\theta}c}{2U}\right)}$$

$$C_{y_\beta} = \frac{\partial C_y}{\partial \beta} \qquad C_{L_\alpha} = \frac{\partial C_L}{\partial \alpha} \qquad \text{etc.}$$

Subscripts:

1,2,3,4 cable numbers (see fig. 12)

F front

R rear

GENERAL REMARKS

Mount System Requirements

Let us consider some general requirements which represent desirable and perhaps essential features in a free-flight mount system (see fig. 1). First, the system should provide a soft support such that the natural frequencies associated with the mount are well below the frequencies of the free-flight rigid body and elastic modes of interest. A soft support implies that the model should be given freedom to respond with large amplitude motions. A second requirement is that moving masses associated with the mount are negligible relative to the total mass of the test article. Also, aerodynamic interference associated with mount structure exposed to the airstream should be low, especially if the system is to be operated at high subsonic or transonic Mach numbers. Another very important requirement is that the system have both static and dynamic stability under all operating conditions. In cases where it is necessary to simulate the steady-state air loads

corresponding to level flight (Froude number simulation), the mount should be capable of applying a steady vertical force to the model which is essentially independent of model motions. Finally, a simple, passive system is preferred over one requiring black boxes or other complex gadgetry in order to meet the above requirements.

Some Typical Systems

Various techniques for mounting dynamic wind-tunnel models have been proposed (see, for example ref. 1). Some typical systems with which the authors are familiar will be discussed with the aid of schematic diagrams shown in figure 2. (Motion pictures illustrating the performance of models utilizing these systems are presented in the oral version of the paper.) The tow-line mount system, described in reference 2, has low aerodynamic interference and provides considerable freedom of motion for the model in all but the longitudinal direction. The major drawback of the system is that a complex, fast-response, autopilot is generally required in order to achieve satisfactory lateral stability and keep the model flying within the confines of the tunnel test section. With the endless wire mount system the model is attached to a vertical wire which passes through pulleys outside of the tunnel to form a continuous loop. While this system has a number of desirable qualities previously mentioned, it was found that models mounted in this way tended to become unstable in yaw. The vertical rod mount system was developed by Boeing Airplane Company and has been used successfully in low-speed wind-tunnel tests for many years (see refs. 3 and 4). At transonic Mach numbers, however, shock waves generated by the rod support become a problem as well as deflections of the rod under high drag loads. The mount system which appears to satisfy the greatest number of the previously mentioned requirements is the two-cable mount, which is the subject of the present paper.

TWO-CABLE MOUNT SYSTEM

Description

The basic two-cable mount system is shown schematically in figure 3. The model is held by two cable loops, one extending to the tunnel walls in the upstream direction and the other in the downstream direction. One loop lies in a vertical plane (either upstream or downstream as best suits the model) and the other loop is in a horizontal plane. Each cable loop passes through pulleys located within the fuselage contour. The cables are kept under tension by stretching a soft spring in the rear cables. The model has freedom to translate horizontally and vertically as well as to rotate in pitch, roll, and yaw. With springs in both cables the model can also be given freedom to translate fore and aft.

Since the model has considerable freedom of motion, it is necessary to provide remote trim controls to keep it centered in the tunnel throughout the test range. Usually only pitch and roll trim control are required. Experience has shown that models can be easily flown by a single operator or

"pilot," using a miniature airplane-type control stick which actuates pitch and roll control surfaces on the model.

Three key parameters that influence the dynamic characteristics of the system shown in figure 3 are:

e distance from front pulleys to center of gravity

a distance from rear pulleys to center of gravity

T_R tension in rear cables

The ability to vary these parameters for a given model provides one with a "handle" by which the stability and flying characteristics of the model can be regulated. The lengths and angles of the cable loops can also be adjusted to satisfy particular requirements. For example, by using unequal angles in the cable loop that lies in a vertical plane, a resultant vertical force may be applied to the model. Since the cables are long (long relative to model deflections) and have tension applied through a soft spring, this resultant vertical force is approximately independent of model motion, and thus provides a reasonable simulation of gravitational forces. By varying tension in the cables steady-state loads on the model can be properly simulated - a feature that may be required when elastic deformations due to steady loads on the aircraft are of importance.

Wind-Tunnel Model

A specific application of the two-cable mount system will now be discussed. Wind-tunnel and theoretical studies of the dynamic characteristics of the mount have been conducted for a model of a modern jet transport. (Similar experience with the present mount system has also been obtained on a supersonic fighter configuration.)

The model, pictured in figures 4 and 5, has a span of approximately 8.5 feet and weighs 70 pounds. It is restrained by a 3/32-inch-diameter forward cable and a 1/16-inch-diameter rear cable through which the tension is applied. Forward and aft pulley locations in the model are $e/c = 1.6$ and $a/c = 0$. When the model is centered in the tunnel, the length of the cables from the model to the wall attachment points is approximately 20 feet; the forward cables are in a vertical plane and the rearward cables in a horizontal plane. The cut-away view in figure 4 gives a schematic indication of the pulley installation. Figure 5 shows the model in a preflight attitude. The large static deflection of the model, which amounts to about 5 feet for the condition shown, is indicative of the softness of the restraining forces involved. Electrical leads for the trim control actuators and accelerometers in the model enter the underside of the fuselage near the center of gravity and are supported at the downstream end by a sting, as can be seen in figures 4 and 5.

Stability Analysis

Equations of motion for the two-cable mount system are derived in the appendix for the general case of six degrees of freedom. Cable-restraining forces are represented in the analysis by a set of stiffness influence coefficients k_{ij} which give the cable force or moment in mode i due to a unit deflection in mode j. Equations for these coefficients in terms of the system parameters are given in table 2. It can be shown that with the assumption of small pertubations from trimmed flight, which make the equations of motion linear, the lateral equations and longitudinal equations for the cable-restrained model are uncoupled and can thus be treated separately as in conventional linearized stability analyses for free-flight conditions (see, for example, ref. 5). Energy dissipation in the pulleys is accounted for by means of an effective viscous damping in each mode.

In the present analysis, a soft spring was assumed to be only in the rear cable, thus the fore-and-aft degree of freedom is suppressed. With this assumption, the dynamic behavior of the system is determined from the roots of a fourth-order characteristic equation for the longitudinal modes and a sixth-order characteristic equation for the lateral modes (see eqs. (12) and (15) in appendix). Tunnel conditions assumed in the analysis are 225 pounds per square foot dynamic pressure and 0.89 Mach number. The aerodynamic derivatives (see table 1) were estimated by the aircraft manufacturer. Damping introduced by the pulleys was assumed to be 5 percent of critical damping for all modes. ($\zeta_n = 0.05$.)

RESULTS AND DISCUSSION

Root-Locus Plots

Before presenting results of the study, it might be appropriate to mention certain features of the root-locus method which will be used to interpret the dynamic characteristics of the system. This method involves plotting roots of the characteristic equation in the complex plane. As shown in figure 6 the imaginary axis indicates the circular frequency of a natural mode and the real axis gives a measure of the damping. The radial distance from the origin to a complex root is the undamped natural frequency ω_n and the angle between the radial vector and the $\pm i\omega$ axis is equal $\sin^{-1}\bar{\zeta}_n$, where $\bar{\zeta}_n$ is the damping ratio relative to critical damping. The system is stable when the real part of every root has a negative sign and is neutrally stable when a root lies on the imaginary axis. A more complete description of the method may be found in reference 5.

Figure 7 shows a typical root-locus plot for the longitudinal modes as tension in the rear cable is varied from 0 to 2.0 times the model weight. (Since the complex roots appear in conjugate pairs, only the upper half of the complex plane is presented.) Shown for comparison is the corresponding short-period mode for free-flight conditions. Note that two oscillatory modes are present for the cable-restrained model. One mode closely corresponds to the free-flight short-period mode and the other is a lightly damped low-frequency

mode which involves primarily vertical translation of the model. This latter mode is associated with the mount restraints and has no counterpart in free flight. The corresponding root-locus plot for the lateral modes is presented in figure 8. Again, both the free-flight and the mount modes are shown. When the model is in free flight, the characteristic equation is of fourth order having one pair of complex conjugate roots and two real roots. The complex roots characterize the Dutch-roll oscillation mode; the real roots are associated with a heavily damped roll mode and an almost neutrally damped spiral mode. When cable restraints are added, the free-flight roots are altered slightly and a new pair of complex conjugate roots comes into the picture. This root involves primarily lateral translation of the model and, as can be seen in figure 8, is unstable except when the tension applied to the rear cable exceeds approximately the weight of the model. These trends are in good qualitative agreement with the experimental results. Motion pictures are available showing the development of lateral instability as cable tension is reduced below $T_R/W = 1.0$.

The root-locus plots given in figures 7 and 8 for various cable tensions are representative of the plots obtained when other parameters are varied in that the free-flight modes are altered slightly and new low-frequency modes are introduced because of the mount restraints. The question of primary interest, then, is whether these mount modes have stable or unstable damping characteristics. Therefore, in the following discussion attention will be focused on the damping ratio associated with the longitudinal and lateral mount modes.

Stability of Mount Modes

Effect of front pulley location.- Figure 9 illustrates the effect of varying the location of the front pulleys when the rear pulleys are at the center of gravity. (See table 1 for values assumed for other parameters in the calculations.) Here it can be seen that the longitudinal mode has satisfactory damping for all conditions; however, the lateral mode for most front pulley locations is unstable when $T_R/W < 1.0$. (Negative values of $\bar{\zeta}$ indicate unstable oscillations.) Note that for zero rear cable tension there is a close correspondence between the present system and the tow-line mount. Thus the requirement for an autopilot to stabilize a tow-line model, such as reference 2, is also evidenced here by the predicted lateral instability shown when $T_R/W = 0$.

Effect of rear pulley location.- Figure 10 indicates the influence of rear pulley location on stability of the mount modes. The front pulleys were assumed to be 1.5c ahead of the center of gravity for these calculations. The parameter being varied, a/c, is taken to be positive when the rear pulleys are aft of the center of gravity. Again, as in the previous case, it is seen that increasing tension in the rear cable has a significant stabilizing influence. Also with tension applied, moving the rear cables aft increases the stability. On the basis of figures 9 and 10 it appears that pulleys equally spaced ahead and behind the c.g. a distance of, say, one mean aerodynamic chord would provide adequate stability over a somewhat larger range of cable-tension values than was possible on the model which had the rear pulleys at the c.g. Equal fore and aft spacing of the pulleys relative

to the c.g. also tends to reduce the coupling between pitch and vertical translation - a feature that may be desired in order to avoid large variations between the no-wind and flight-attitude angle of the model.

Effect of static margin.- In the previously discussed results it was found both analytically and experimentally that the longitudinal mount mode was stable for all conditions considered. Let us now examine analytically how longitudinal stability is influenced by changes in the static margin of the model. The static margin, defined as the distance between the stick-fixed neutral point and the c.g. of the model in mean aerodynamic chords, was varied by moving the c.g. and at the same time the pulley locations such that $e/c = 1.5$ and $a/c = 0$. Variations in the moment of inertia due to c.g. changes were neglected. The results are given in figure 11. Note that as the c.g. is moved aft the stability of the mount mode falls off rather abruptly for all values of cable tension considered. (The nominal c.g. location used in other cases was 0.25c giving a static margin of 0.263c.) Thus it might be concluded that configurations having a small margin of static stability in free flight are likely to develop instabilities when restrained by cables in a wind tunnel.

CONCLUDING REMARKS

It has been shown that by means of a rather simple two-cable mount system the free-flight rigid-body modes of complete aircraft can be closely simulated in a wind tunnel. A stability analysis and wind-tunnel evaluation of the system indicate that by proper selection of such parameters as cable tension and pulley spacing, stable dynamic behavior of the mount can be achieved over a broad range of test conditions. In addition to flutter and gust response applications, the system offers potential as a research tool for measuring stability derivatives and maneuver loads on complete aeroelastic models.

APPENDIX

STABILITY ANALYSIS OF CABLE MOUNT SYSTEM

Consider the cable configuration shown schematically in figure 12. The x, y, and z axes form a right-hand set of space-fixed orthogonal coordinates with the origin at the center of gravity of the model in steady trimmed flight. The model is assumed to be rigid so that its motion is completely described by six degrees of freedom - namely, x, y, and z translations of the center of gravity and φ, θ, ψ rotations about the x, y, and z axes, respectively. The equations of motion are linearized by the assumption of small pertubations from trimmed flight. Inertia and vibratory characteristics of the restraining cables are neglected.

The dynamical equations of motion for the system can be written as follows:

Longitudinal translation:

$$X_C + X_A = m\ddot{x} \tag{1a}$$

Lateral translation:

$$Y_C + Y_A = m\ddot{y} \tag{1b}$$

Vertical translation:

$$Z_C + Z_A + mg = m\ddot{z} \tag{1c}$$

Roll:

$$L_C + L_A = r_x^2 m\ddot{\varphi} - I_{xz}\ddot{\psi} \tag{1d}$$

Pitch:

$$M_C + M_A = r_y^2 m\ddot{\theta} \tag{1e}$$

Yaw:

$$N_C + N_A = r_z^2 m\ddot{\psi} - I_{xz}\ddot{\varphi} \tag{1f}$$

Where the C and A subscripts denote cable and aerodynamic terms, respectively.

Cable Restraints

As shown in figure 12 the particular cable configuration chosen for analysis has the forward cables in a vertical plane and the rearward cables in a horizontal plane. Tension is applied to the cables by stretching a soft spring in the rear cable. It has been assumed that in trimmed flight

the rear cables are symmetrical with respect to the plane of symmetry of the model; however, in order to permit the possibility of applying a steady-state vertical force to the model, the cable angle of the upper front cable β_1 is not necessarily the same as that of the lower front cable β_2.

The total forces and moment about the center of gravity are obtained by summing the contribution of each of the four cables:

$$X_C = X_{C1} + X_{C2} + X_{C3} + X_{C4} \tag{2a}$$

$$Y_C = Y_{C1} + Y_{C2} + Y_{C3} + Y_{C4} \tag{2b}$$

$$Z_C = Z_{C1} + Z_{C2} + Z_{C3} + Z_{C4} \tag{2c}$$

$$\begin{aligned} L_C = {} & (h + e\bar{\theta})Y_{C1} - (h - e\bar{\theta})Y_{C2} - (a\bar{\theta} - d\varphi)Y_{C3} - (a\bar{\theta} + d\varphi)Y_{C4} \\ & + (h\varphi + e\psi)Z_{C1} - (h\varphi - e\psi)Z_{C2} - (d + a\psi)Z_{C3} + (d - a\psi)Z_{C4} \end{aligned} \tag{2d}$$

$$\begin{aligned} M_C = {} & -(h + e\bar{\theta})X_{C1} + (h - e\bar{\theta})X_{C2} + (a\bar{\theta} - d\varphi)X_{C3} + (a\bar{\theta} + d\varphi)X_{C4} \\ & + (h\bar{\theta} - e)Z_{C1} - (h\bar{\theta} + e)Z_{C2} + (a - d\psi)Z_{C3} + (a + d\psi)Z_{C4} \end{aligned} \tag{2e}$$

$$\begin{aligned} N_C = {} & -(e\psi + h\varphi)X_{C1} - (e\psi - h\varphi)X_{C2} + (d + a\psi)X_{C3} - (d - a\psi)X_{C4} \\ & + (e - h\bar{\theta})Y_{C1} + (e + h\bar{\theta})Y_{C2} + (d\psi - a)Y_{C3} - (d\psi + a)Y_{C4} \end{aligned} \tag{2f}$$

where $\bar{\theta} = \theta_o + \theta$. The x, y, and z components of tension in each cable are assumed to act at the outermost point of tangency between the cable and its pulley, and the model center of gravity is assumed to be on the line formed by the intersection of the planes of symmetry of the front and rear pulleys. From the geometry of the situation, these force components can be expressed:

$$\left.\begin{array}{lll} X_{C1} = T_F \cos \beta_1, & Y_{C1} = -T_F \dfrac{y_1}{l_1}, & Z_{C1} = -T_F \sin \beta_1 \\ X_{C2} = T_F \cos \beta_2, & Y_{C2} = -T_F \dfrac{y_2}{l_2}, & Z_{C2} = T_F \sin \beta_2 \\ X_{C3} = T_R \cos \beta_3, & Y_{C3} = -T_R \sin \beta_3, & Z_{C3} = -T_R \dfrac{z_3}{l_3} \\ X_{C4} = -T_R \cos \beta_4, & Y_{C4} = T_R \sin \beta_4, & Z_{C4} = -T_R \dfrac{z_4}{l_4} \end{array}\right\} \tag{3}$$

The terms on the right-hand side of equations (3) consist of a steady-state part plus increments proportional to motions of the model. By way of illustration consider the vertical component of force on pulley number 1 (see eqs. (3) and fig. 12).

$$Z_{C1} = -T_F \sin \beta_1$$

which can be written

$$\begin{aligned} Z_{C1} &= Z_{C1_o} + \Delta Z_{C1} \\ &= T_F \sin \beta_1 - \Delta T_F \sin \beta_1 - \Delta\beta_1 T_F \cos \beta_1 \end{aligned} \tag{4}$$

The increments ΔT_F and $\Delta\beta_1$ can, in turn, be expressed in terms of pertubations of the model center of gravity as follows:

$$\begin{aligned} \Delta T_F &= k_F\left(\Delta l_1 + \Delta l_2\right) \\ &= k_F\left[\left(z_1 \sin \beta_1 - x_1 \cos \beta_1\right) - \left(z_2 \cos \beta_2 + x_2 \cos \beta_2\right)\right] \end{aligned} \tag{5}$$

and

$$\Delta\beta_1 = \frac{x_1}{l_1} \sin \beta_1 + \frac{z_1}{l_1} \cos \beta_1 \tag{6}$$

where x_n and z_n denote components of displacement of the outermost points of cable tangency on pulley n

$$\left.\begin{aligned} x_1 &= x - h\bar{\theta}, & z_1 &= z - e\bar{\theta} \\ x_2 &= x + h\bar{\theta}, & z_2 &= z + e\bar{\theta} \end{aligned}\right\} \tag{7}$$

Thus, with equations (5), (6), and (7) substituted into equation (4) the vertical-force component on pulley 1 can be written in the form

$$Z_{C1} = Z_{C1_o} - k_{zx_1}x - k_{zz_1}z - k_{z\theta_1}\theta \tag{8}$$

where the coefficients k_{ij_1} are stiffness-influence coefficients associated with the upper front cable which goes to pulley 1. In a similar manner the three components of cable force are derived for each of the four pulleys. When these relations are substituted into equations (2) and all terms involving products of the pertubations x, y, z, φ, θ, and ψ discarded, the following set of linear relations are obtained for cable restraints on the overall system:

$$X_C = X_{C_o} - k_{xx}x - k_{xz}z - k_{x\theta}\theta \tag{9a}$$

$$Y_C = -k_{yy}y - k_{y\varphi}\varphi - k_{y\psi}\psi \tag{9b}$$

$$Z_C = Z_{C_o} - k_{zx}x - k_{zz}z - k_{z\theta}\theta \tag{9c}$$

$$L_C = -k_{\varphi y}y - k_{\varphi\varphi}\varphi - k_{\varphi\psi}\psi \tag{9d}$$

$$M_C = M_{C_o} - k_{\theta x}x - k_{\theta z}z - k_{\theta\theta}\theta \tag{9e}$$

$$N_C = -k_{\psi y}y - k_{\psi\varphi}\varphi - k_{\psi\psi}\psi \tag{9f}$$

Equations for the steady-state terms and the influence coefficients appearing in equations (9) are given in table 2.

It is important to note in equations (9) that the cable restraints produce no coupling between the longitudinal modes (x, z, and θ) and the lateral modes (y, φ, and ψ). Thus, if the lateral and longitudinal modes of an aircraft configuration can be isolated and studied separately for free-flight conditions, as is most generally done in linearized stability analyses, the same simplifications can also be enjoyed for the cable-supported model. The assumption of separable longitudinal and lateral modes will be made throughout the remainder of the present analysis.

Aerodynamic Forces and Moments

For small pertubations from the space-fixed axes considered herein and with the assumption $\dot{x}/U, \dot{y}/U, \dot{z}/U \ll 1.0$, the aerodynamic forces and moments about the center of gravity of the model can be expressed as follows:

Longitudinal modes:

$$X_A = -qS\left[\left(C_{D_o} + C_{D_\alpha}\theta_o\right) + 2\left(C_{D_o} + C_{D_\alpha}\theta_o\right)\frac{\dot{x}}{U} + \left(C_{D_\alpha} - C_{L_o} - C_{L_\alpha}\theta_o - C_{L_\delta}\delta_o\right)\frac{\dot{z}}{U} + C_{D_\alpha}\theta\right] \tag{10a}$$

$$Z_A = -qS\left[\left(C_{L_o} + C_{L_\alpha}\theta_o + C_{L_\delta}\delta_o\right) + 2\left(C_{L_o} + C_{L_\alpha}\theta_o + C_{L_\delta}\delta_o\right)\frac{\dot{x}}{U} + \left(C_{L_\alpha} + C_{D_o} + C_{D_\alpha}\theta_o\right)\frac{\dot{z}}{U} + C_{L_\alpha}\theta\right] \tag{10b}$$

$$M_A = -qSc\left[\left(C_{m_o} + C_{m_\alpha}\theta_o + C_{m_\delta}\delta_o\right) + 2\left(C_{m_o} + C_{m_\alpha}\theta_o + C_{m_\delta}\delta_o\right)\frac{\dot{x}}{U} + C_{m_\alpha}\frac{\dot{z}}{U} + \frac{c}{2U}C_{m_\alpha}\frac{\ddot{z}}{U} + C_{m_\alpha}\theta + \frac{c}{2U}\left(C_{m_{\dot{\alpha}}} + C_{m_q}\right)\dot{\theta}\right] \tag{10c}$$

Lateral modes:

$$Y_A = qS\left[\left(C_{y_\beta} - C_{D_o} - C_{D_\alpha}\theta_o\right)\frac{\dot{y}}{U} + \left(C_{L_o} + C_{L_\alpha}\theta_o + C_{L_\delta}\delta_o\right)\varphi + C_{y_p}\frac{b}{2U}\dot{\varphi} - C_{y_\beta}\psi + C_{y_r}\frac{b}{2U}\dot{\psi}\right] \tag{11a}$$

$$L_A = qSb\left(C_{l_\beta}\frac{\dot{y}}{U} + C_{l_p}\frac{b}{2U}\dot{\Phi} - C_{l_\beta}\Psi + C_{l_r}\frac{b}{2U}\dot{\Psi}\right) \tag{11b}$$

$$N_A = qSb\left(C_{n_\beta}\frac{\dot{y}}{U} + C_{n_p}\frac{b}{2U}\dot{\Phi} - C_{n_\beta}\Psi + C_{n_r}\frac{b}{2U}\dot{\Psi}\right) \tag{11c}$$

With the cable terms defined by equations (9) and the aerodynamic terms by equations (10) and (11), the equations of motion for the cable mount system become a set of linear second-order differential equations with constant coefficients. In writing out the final form of these equations, it was found convenient to divide each equation through by an appropriate inertia. In addition, energy dissipation in the pulleys has been represented by an effective viscous damping ratio ζ_i for each mode.

Linearized Equations of Motion

The equations of motion expressed in Laplace transform notation are:

Longitudinal modes:

$$\left(s^2 + a_{11}s + a_{10}\right)x(s) + \left(b_{11}s + b_{10}\right)z(s) + c_{10}\theta(s) = \frac{X_o}{m} \tag{12a}$$

$$\left(a_{21}s + a_{20}\right)x(s) + \left(s^2 + b_{21}s + b_{20}\right)z(s) + c_{20}\theta(s) = \frac{Z_o}{m} \tag{12b}$$

$$\left(a_{31}s + a_{30}\right)x(s) + \left(b_{32}s^2 + b_{31}s + b_{30}\right)z(s) + \left(s^2 + c_{31}s + c_{30}\right)\theta(s) = \frac{M_o}{mr_y^2} \tag{12c}$$

where

$$a_{11} = 2\zeta_x\omega_{xx} + 2\sigma\left(C_{D_o} + C_{D_\alpha}\theta_o\right) \qquad b_{11} = \sigma\left(C_{D_\alpha} - C_{L_o} - C_{L_\alpha}\theta_o - C_{L_\delta}\delta_o\right) \qquad c_{10} = \omega_{x\theta}^2 + U\sigma C_{D_\alpha}$$

$$a_{10} = \omega_{xx}^2 \qquad b_{10} = \omega_{xz}^2 \qquad c_{20} = \omega_{z\theta}^2 + U\sigma C_{L_\alpha}$$

$$a_{21} = 2\sigma\left(C_{L_o} + C_{L_\alpha}\theta_o + C_{L_\delta}\delta_o\right) \qquad b_{21} = 2\zeta_z\omega_z + \sigma\left(C_{D_o} + C_{D_\alpha}\theta_o + C_{L_\alpha}\right) \qquad c_{31} = \frac{2\zeta_\theta\omega_{\theta\theta}}{r_y} - \frac{c^2\sigma}{2r_y^2}\left(C_{m_{\dot\alpha}} + C_{m_q}\right)$$

$$a_{20} = \omega_{zx}^2 \qquad b_{20} = \omega_{zz}^2 \qquad c_{30} = \frac{\omega_{\theta\theta}^2}{r_y^2} - \frac{U\sigma C}{r_y^2} C_{m_\alpha}$$

$$a_{31} = -\frac{2c\sigma}{r_y^2}\left(C_{m_o} + C_{m_\alpha}\theta_o + C_{m_\delta}\delta_o\right) \qquad b_{31} = -\frac{c\sigma}{r_y^2} C_{m_\alpha}$$

$$a_{30} = \frac{\omega_{\theta x}^2}{r_y^2} \qquad b_{30} = \frac{\omega_{\theta z}^2}{r_y^2}$$

$$b_{32} = -\frac{c^2\sigma}{2r_y^2 U} C_{m_{\dot\alpha}}$$

and

$$X_o = -qS\left(C_{D_o} + C_{D_\alpha}\theta_o\right) + X_{C_o} \qquad \sigma = \frac{\rho US}{2m}$$

$$Z_o = -qS\left(C_{L_o} + C_{L_\alpha}\theta_\sigma + C_{L_\delta}\delta_o\right) \qquad \omega_{ij}^2 = \frac{k_{ij}}{m}$$

$$M_o = +qSc\left(C_{m_o} + C_{m_\alpha}\theta_o + C_{m_\delta}\delta_o\right) + M_{C_o} \qquad \zeta_i = \text{Effective viscous damping ratio of mount for mode } i$$

The terms on the right-hand side of equations (12) are the static aerodynamic and cable restraint forces and moments acting on the model. They are defined

$$X_o = X_{C_o} + X_{A_o} = \frac{T_F}{m}\left(\cos \beta_1 + \cos \beta_2\right) - 2\frac{T_R}{m}\cos \beta_3 - \omega_{x\theta}^2 \theta_o - U\sigma\left(C_{D_o} + C_{D_\alpha}\theta_o\right) \tag{13a}$$

$$Z_o = Z_{C_o} + Z_{A_o} = \frac{T_F}{m}\left(\sin \beta_2 - \sin \beta_1\right) - \omega_{z\theta}^2 \theta_o + g - U\sigma\left(C_{L_o} + C_{L_\alpha}\theta_o + C_{L_\delta}\delta_o\right) \tag{13b}$$

$$M_o = M_{C_o} + M_{A_o} = \frac{eT_F}{r_y{}^2 m}\left(\sin \beta_1 - \sin \beta_2 - \frac{h}{e}\cos \beta_1 + \frac{h}{e}\cos \beta_2\right) - \frac{\omega_{\theta\theta}^2 \theta_o}{r_y{}^2} + \frac{U\sigma c}{r_y{}^2}\left(C_{m_o} + C_{m_\alpha}\theta_o + C_{m_\delta}\delta_o\right) \tag{13c}$$

These equations set equal to zero define the conditions on T_F, θ_o, and δ_o which must be simultaneously satisfied in steady trimmed flight with specified tension in the rear cables. (T_F and θ_o are required to evaluate the cable influence coefficients in table 2.) In most instances it is not necessary to know precise values for T_F, θ_o, and δ_o and they may therefore be calculated independently in the following approximate manner:

In equation (13a) neglect θ_o and solve for T_F

$$T_F = 2T_R\left(\frac{\cos \beta_3}{\cos \beta_1 + \cos \beta_2}\right) + \frac{mU\sigma C_{D_o}}{\cos \beta_1 + \cos \beta_2} \tag{14a}$$

In equation (13b) neglect δ_o and θ_o and, with T_F as given by equation (14a), solve for θ_o

$$\theta_o = \frac{1}{U\sigma C_{L_\alpha}}\left[\frac{T_F}{m}\left(\sin \beta_2 - \sin \beta_1\right) + g\right] - \frac{C_{L_o}}{C_{L_\alpha}} \tag{14b}$$

From equation (13c) solve for the remaining unknown δ_o

$$\delta_o = -\frac{eT_F}{mcU\sigma C_{m_\delta}}\left(\sin \beta_1 - \sin \beta_2 - \frac{h}{e}\cos \beta_1 + \frac{h}{e}\cos \beta_2\right) - \frac{C_{m_o} + C_{m_\alpha}\theta_o}{C_{m_\delta}} \tag{14c}$$

(Note from the latter two equations that when $\beta_1 = \beta_2$ the cable restraints do not affect θ_o or δ_o.)

Lateral equations:

$$\left(s^2 + \bar{a}_{11}s + \bar{a}_{10}\right)y(s) + \left(\bar{b}_{11}s + \bar{b}_{10}\right)\varphi(s) + \left(\bar{c}_{11}s + \bar{c}_{10}\right)\psi(s) = 0 \tag{15a}$$

$$\left(\bar{a}_{21}s + \bar{a}_{20}\right)y(s) + \left(s^2 + \bar{b}_{21}s + \bar{b}_{20}\right)\varphi(s) + \left(\bar{c}_{22}s^2 + \bar{c}_{21}s + \bar{c}_{20}\right)\psi(s) = 0 \tag{15b}$$

$$\left(\bar{a}_{31}s + \bar{a}_{30}\right)y(s) + \left(\bar{b}_{32}s^2 + \bar{b}_{31}s + \bar{b}_{30}\right)\varphi(s) + \left(s^2 + \bar{c}_{31}s + \bar{c}_{30}\right)\psi(s) = 0 \tag{15c}$$

where

$$\bar{a}_{11} = 2\zeta_y\omega_{yy} - \sigma\left(C_{y_\beta} - C_{D_o} - C_{D_\alpha}\theta_o\right) \qquad \bar{b}_{11} = -\frac{b}{2}\sigma C_{y_p} \qquad \bar{c}_{11} = -\frac{b}{2}\sigma C_{y_r}$$

$$\bar{a}_{10} = \omega_{yy}^2 \qquad \bar{b}_{10} = \omega_{y\varphi}^2 - U\sigma\left(C_{L_o} + C_{l_\alpha}\theta_o + C_{L_\delta}\delta_o\right) \qquad \bar{c}_{10} = \omega_{y\psi}^2 + U\sigma C_{y_\beta}$$

$$\bar{a}_{21} = -\frac{b}{r_x^2}\sigma C_{l_\beta} \qquad \bar{b}_{21} = 2\zeta_\varphi\frac{\omega_{\varphi\varphi}}{r_x} - \frac{b^2}{2r_x^2}\sigma C_{l_p} \qquad \bar{c}_{22} = -\frac{I_{xz}}{mr_x^2}$$

$$\bar{a}_{20} = \frac{\omega_{\varphi y}^2}{r_x^2} \qquad \bar{b}_{20} = \frac{\omega_{\varphi\varphi}^2}{r_x^2} \qquad \bar{c}_{21} = -\frac{b^2}{2r_x^2}\sigma C_{l_r}$$

$$\bar{a}_{31} = -\frac{b}{r_z^2}\sigma C_{n_\beta} \qquad \bar{b}_{32} = -\frac{I_{xz}}{mr_z^2} \qquad \bar{c}_{20} = \frac{\omega_{\varphi\psi}^2}{r_x^2} + \frac{Ub\sigma}{r_x^2}C_{l_\beta}$$

$$\bar{a}_{30} = \frac{\omega_{\psi y}^2}{r_z^2} \qquad \bar{b}_{31} = -\frac{b^2}{2r_z^2}\sigma C_{n_p} \qquad \bar{c}_{31} = \frac{2\zeta_\psi\omega_{\psi\psi}}{r_z} - \frac{b^2}{2r_z^2}\sigma C_{n_r}$$

$$\bar{b}_{30} = \frac{\omega_{\psi\varphi}^2}{r_z^2} \qquad \bar{c}_{30} = \frac{\omega_{\psi\psi}^2}{r_z^2} + \frac{bU}{r_z^2}\sigma C_{n_\beta}$$

Lateral and longitudinal stability of the system is determined from roots of the characteristic equations obtained by setting the determinant of the coefficients in equations (12) and (15) equal to zero. These roots appear as complex conjugate pairs ($s = \eta \pm i\omega$) for the oscillatory modes and as pure real numbers ($s = \eta$) for the aperiodic modes. In either case the system is stable when $\eta < 0$, neutrally stable when $\eta = 0$, and unstable when $\eta > 0$.

REFERENCES

1. Bisplinghoff, R. L., Ashley, H., and Halfman, R. L.: Aeroelasticity. Addison-Wesley Pub. Co., Inc., 1955, pp. 791-800.

2. Schneider, W. C.: Development of a New Flutter Testing Technique Using a Towed Dynamic Airplane Model Equipped With an Automatic Stabilizing System. NACA RM L54L23, 1954.

3. Kinnaman, E. B.: Flutter Analysis of Complex Airplanes by Experimental Methods. Jour. Aero. Sci., vol. 19, no. 9, Sept. 1952.

4. Abbott, F. T., Jr., Kelly, H. N., and Hampton, K. D.: Investigation of Propeller-Power-Plant Autoprecession Boundaries for a Dynamic-Aeroelastic Model of a Four-Engine Turboprop Transport Airplane. NASA TN D-1806, 1963.

5. Etkin, B.: Dynamics of Flight, Stability and Control. John Wiley & Son, Inc., 1959.

TABLE 1.- CONDITIONS ASSUMED FOR STABILITY ANALYSIS

Physical properties of model:	
Weight, W, lb	70.0
Wing span, b, ft	8.46
Wing area, S, sq ft	8.94
Mean aerodynamic chord, c, ft	1.168
Moments of inertia:	
$I_x = mr_x^2$, slug-ft^2	5.25
$I_y = mr_y^2$, slug-ft^2	2.59
$I_z = mr_z^2$, slug-ft^2	7.30
I_{xz}, slug-ft^2	0
Center-of-gravity location (nominal)	0.25c
Stick fixed neutral point, N	0.513c
Aerodynamic derivatives:	
C_{L_o}	0.035
C_{D_o}	0.02
C_{D_α}	0.34
C_{L_α}	4.64
C_{m_α} (nominal)	-1.22
$C_{m_{\dot{\alpha}}}$	-3.85
C_{m_q}	-15.65
θ_o	0
C_{y_β}	-0.725
C_{y_p}	0.105
C_{y_r}	0.0051
C_{l_β}	-0.0617
C_{l_p}	-0.401
C_{l_r}	0.078
C_{n_β}	0.117
C_{n_p}	-0.0199
C_{n_r}	-0.124
Test conditions:	
Test medium	Freon 12
Dynamic pressure, q, lb/sq ft	225.0

TABLE 1.- CONDITIONS ASSUMED FOR STABILITY ANALYSIS - Concluded

Mach number	0.89
Velocity, U, ft/sec	470
$\sigma = \frac{\rho US}{2m}$, sec^{-1}	1.98
Mount system parameters:	
Cable length, $l_1 = l_2 = l_3 = l_4 =$, ft	20.0
Cable angles, $\beta_1 = \beta_2 = \beta_3 = \beta_4 =$, deg	20.0
Front pulley separation distance, 2h, ft	0.70
Rear pulley separation distance, 2d, ft	0.60
Pulley damping ratio, ζ_n (all modes)	0.05
Front cable tension, T_F, lb	$T_R + 21.4$
Rear cable tension, T_R, lb	$0 \leqq T_R \leqq 140$
Distance between center of gravity and front pulleys, e	$0 \leqq \frac{e}{c} \leqq 2.0$
Distance between center of gravity and rear pulleys, a	$-0.5c \leqq \frac{a}{c} \leqq 1.0$
Spring constant in rear cable, k_R, lb/in.	5.0

TABLE 2.- CABLE INFLUENCE COEFFICIENTS

[See eqs. (9)]

Longitudinal force:

$$X_{C_o} = T_F\left(\cos \beta_1 + \cos \beta_2\right) - 2T_R \cos \beta_R - k_{x\theta}\theta_o$$

$$k_{xx} = \frac{T_F}{l_1} \sin^2\beta_1 + \frac{T_F}{l_2} \sin^2\beta_2 + \frac{2T_R}{l_R} \sin^2\beta_R + k_F\left(\cos \beta_1 + \cos \beta_2\right)^2 + 4k_R \cos^2\beta_R$$

$$k_{xz} = \frac{T_F}{l_1} \cos \beta_1 \sin \beta_1 - \frac{T_F}{l_2} \cos \beta_2 \sin \beta_2$$

$$- k_F\left(\cos \beta_1 + \cos \beta_2\right)\left(\sin \beta_1 - \sin \beta_2\right)$$

$$k_{x\theta} = - \frac{T_F}{l_1} \sin \beta_1\left(h \sin \beta_1 + e \cos \beta_1\right) + \frac{T_F}{l_2} \sin \beta_2\left(h \sin \beta_2 + e \cos \beta_2\right)$$

$$- k_F\left(\cos \beta_1 + \cos \beta_2\right)\left[e\left(\sin \beta_2 - \sin \beta_1\right) + h\left(\cos \beta_1 - \cos \beta_2\right)\right]$$

Lateral force:

$$k_{yy} = \frac{T_F}{l_1} + \frac{T_F}{l_2} + \frac{2T_R}{l_R} \cos^2\beta_R$$

$$k_{y\varphi} = T_F\left(\frac{h}{l_1} - \frac{h}{l_2}\right)$$

$$k_{y\psi} = T_F\left(\frac{e}{l_1} + \frac{e}{l_2}\right) - \frac{2T_R \cos \beta_R}{l_R}\left(d \sin \beta_R + a \cos \beta_R\right)$$

Vertical force:

$$Z_{C_o} = T_F\left(\sin \beta_2 - \sin \beta_1\right) - k_{z\theta}\theta_o$$

$$k_{zx} = k_{xz}$$

$$k_{zz} = \frac{T_F}{l_1} \cos^2\beta_1 + \frac{T_F}{l_2} \cos^2\beta_2 + \frac{2T_R}{l_R} + k_F\left(\sin \beta_2 - \sin \beta_1\right)^2$$

TABLE 2.- CABLE INFLUENCE COEFFICIENTS - Continued

$$k_{z\theta} = -T_F h\left(\frac{\sin\beta_1 \cos\beta_1}{l_1} + \frac{\sin\beta_2 \cos\beta_2}{l_2}\right) - T_F e\left(\frac{\cos^2\beta_1}{l_1} + \frac{\cos^2\beta_2}{l_2}\right) + 2T_R \frac{a}{l_R}$$

$$- k_F(\sin\beta_2 - \sin\beta_1)\left[e(\sin\beta_2 - \sin\beta_1) - h(\cos\beta_2 - \cos\beta_1)\right]$$

Roll:

$$k_{\varphi y} = k_{y\varphi}$$

$$k_{\varphi\varphi} = hT_F\left(\frac{h}{l_1} + \frac{h}{l_2} + \sin\beta_1 + \sin\beta_2\right) + 2dT_R\left(\frac{d}{l_R} + \sin\beta_R\right)$$

$$k_{\varphi\psi} = hT_F\left(\frac{e}{l_1} - \frac{e}{l_2}\right) + T_F e(\sin\beta_1 - \sin\beta_2)$$

Pitch:

$$M_{C_o} = eT_F(\sin\beta_1 - \sin\beta_2) - hT_F(\cos\beta_1 - \cos\beta_2) - k_{\theta\theta}\theta_o$$

$$k_{\theta x} = k_{x\theta}$$

$$k_{\theta z} = k_{z\theta}$$

$$k_{\theta\theta} = T_F\left[l_1\left(\frac{e}{l_1}\cos\beta_1 + \frac{h}{l_1}\sin\beta_1\right)^2 + \frac{l}{l_2}(e\cos\beta_2 + h\sin\beta_2)^2 + h(\sin\beta_1\right.$$

$$\left. + \sin\beta_2) + e(\cos\beta_1 + \cos\beta_2)\right] + 2T_R\, a\cos\beta_R + k_F\left[e(\sin\beta_2 - \sin\beta_1)\right.$$

$$\left. + h(\cos\beta_1 - \cos\beta_2)\right]^2 + \frac{2a^2 T_R}{l_R}$$

TABLE 2.- CABLE INFLUENCE COEFFICIENTS - Concluded

Yaw:

$$k_{\psi y} = k_{y\psi}$$

$$k_{\psi\varphi} = hT_F\left(\frac{e}{l_1} - \frac{e}{l_2} + \cos\beta_1 - \cos\beta_2\right)$$

$$k_{\psi\psi} = eT_F\left(\frac{e}{l_1} + \frac{e}{l_2} + \cos\beta_1 + \cos\beta_2\right) + 2T_R\left[a\cos\beta_R + d\sin\beta_R + \frac{1}{l_R}(a\cos\beta_R + d\sin\beta_R)^2\right]$$

- SOFT SUPPORT
- NEGLIGIBLE MASS
- LOW AERODYNAMIC INTERFERENCE
- STABLE
- SIMPLE

NASA

Figure 1.- Mount requirements.

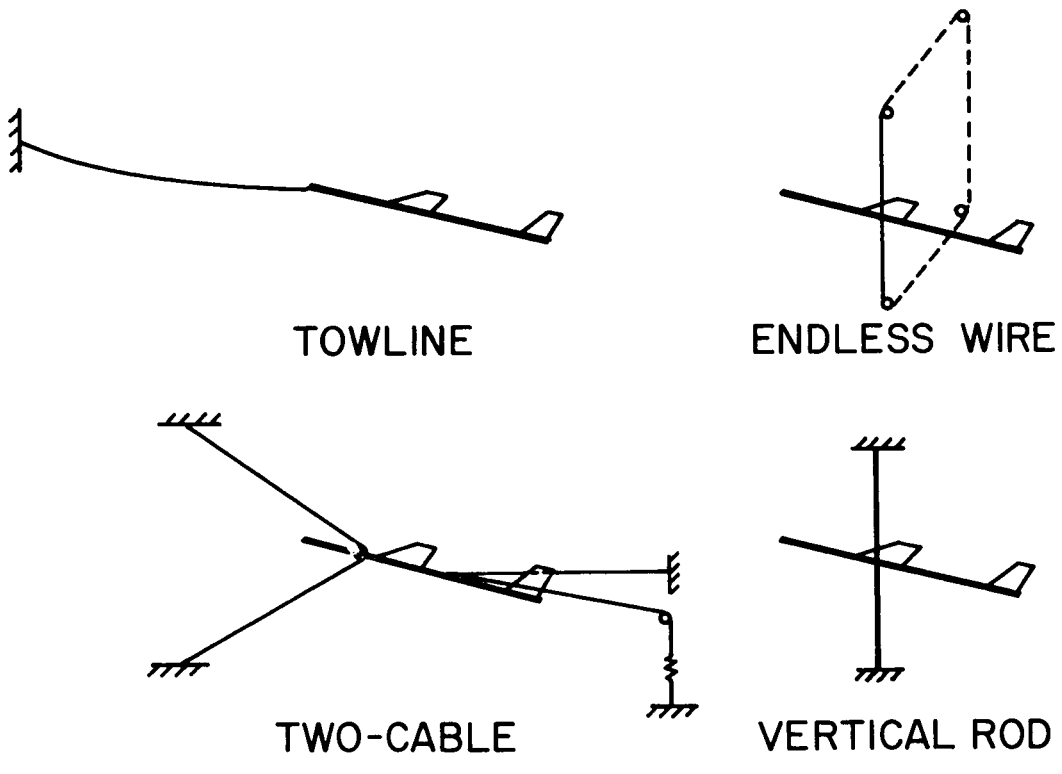

NASA

Figure 2.- Free-flight mount systems.

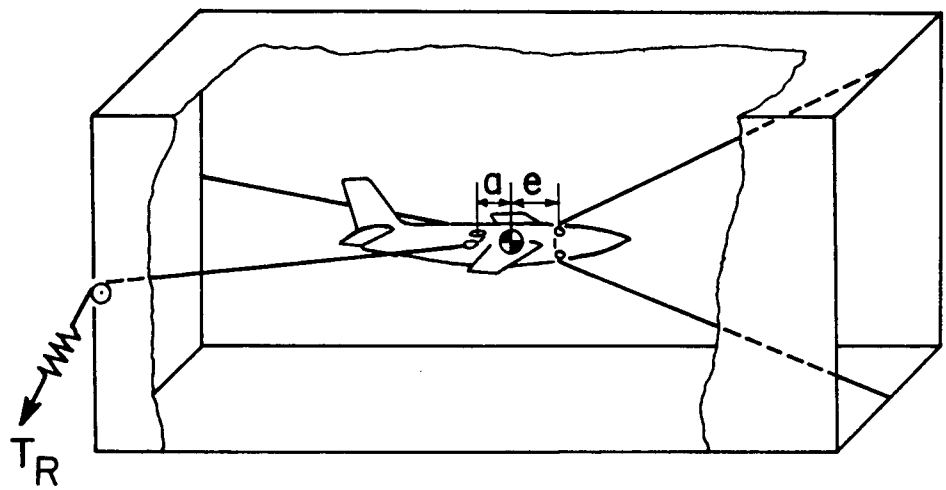

NASA

Figure 3.- Two-cable mount.

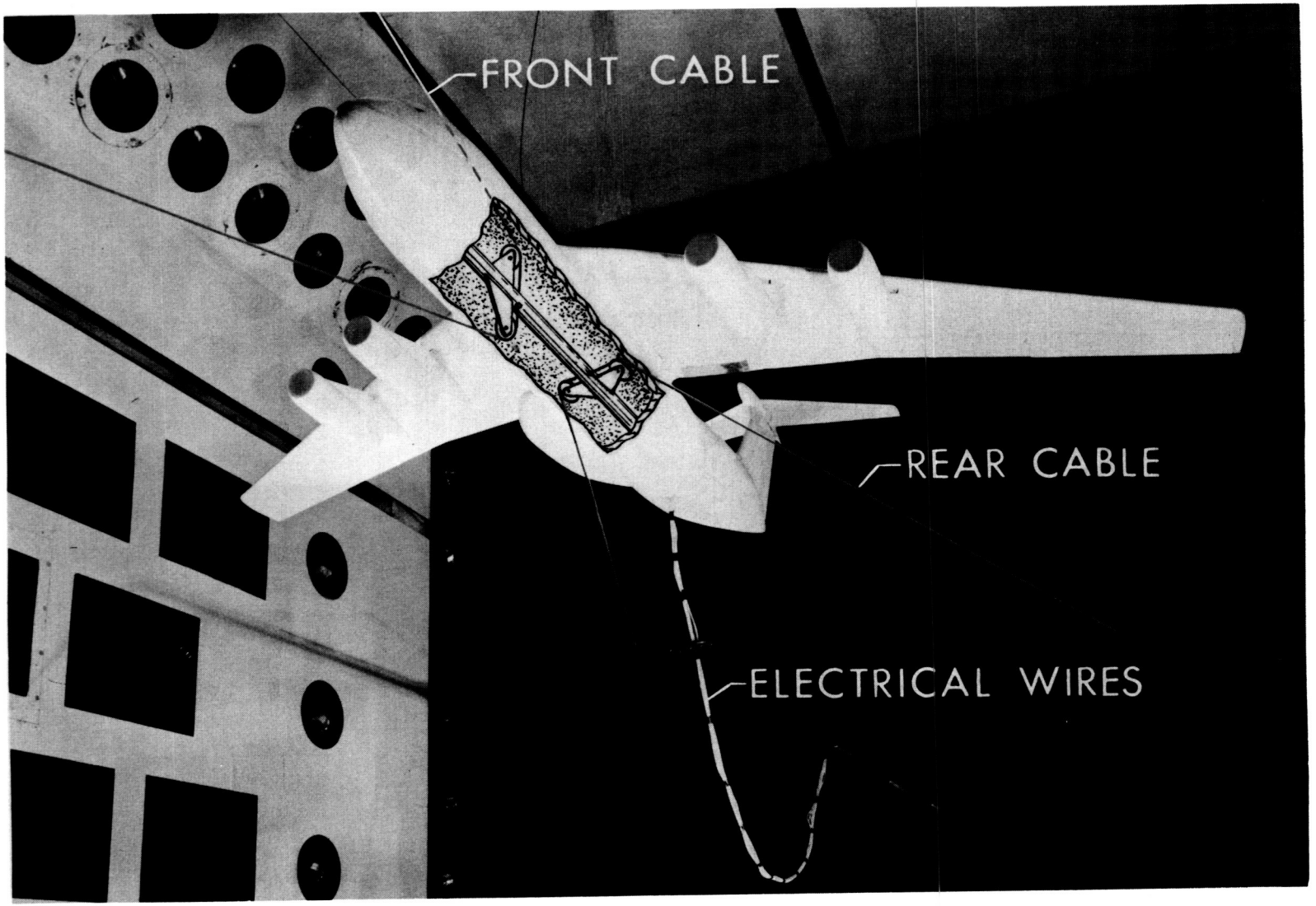

NASA

Figure 4.- Model on two-cable mount.

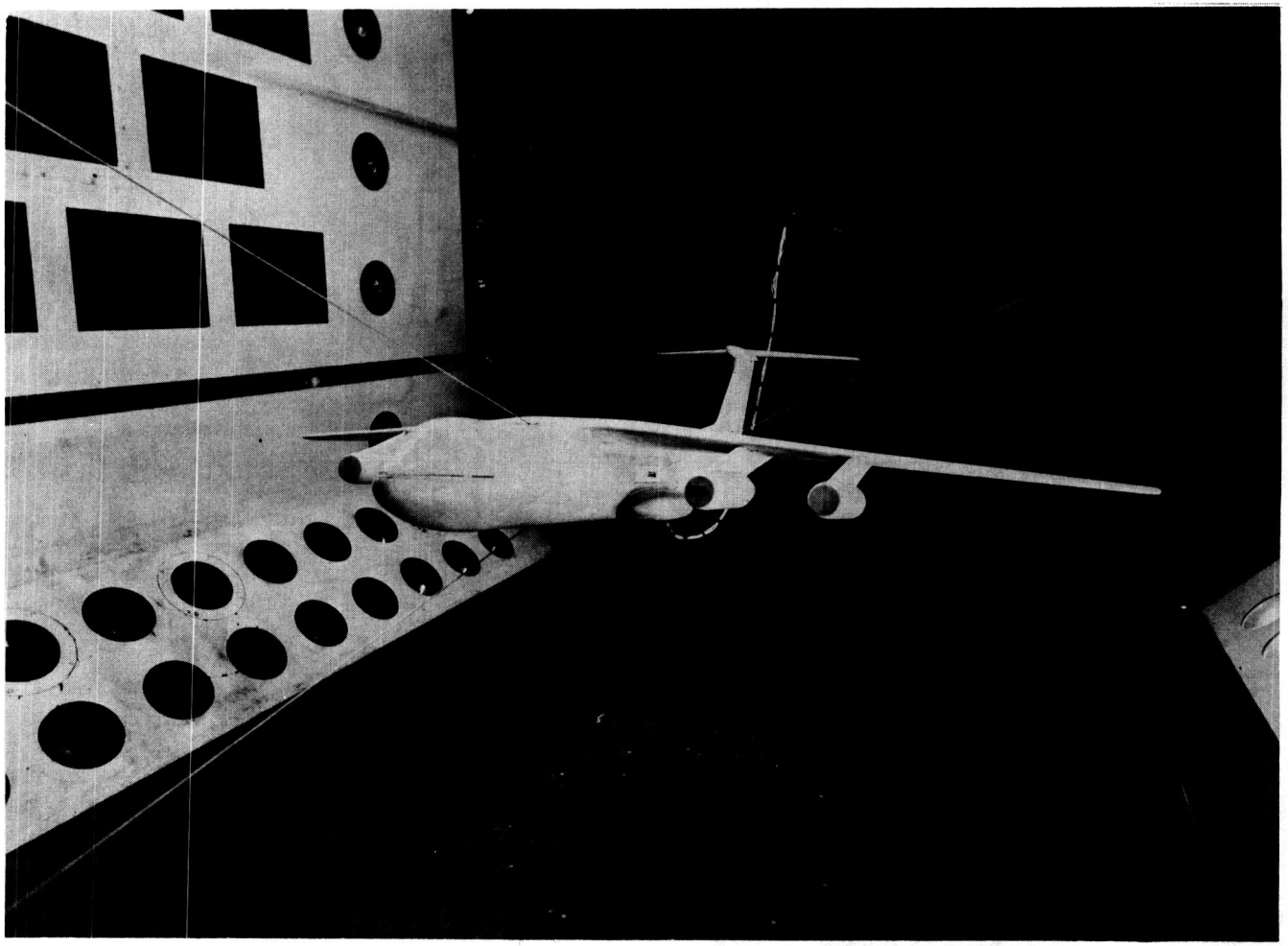

NASA

Figure 5.- Cable mounted model in preflight attitude.

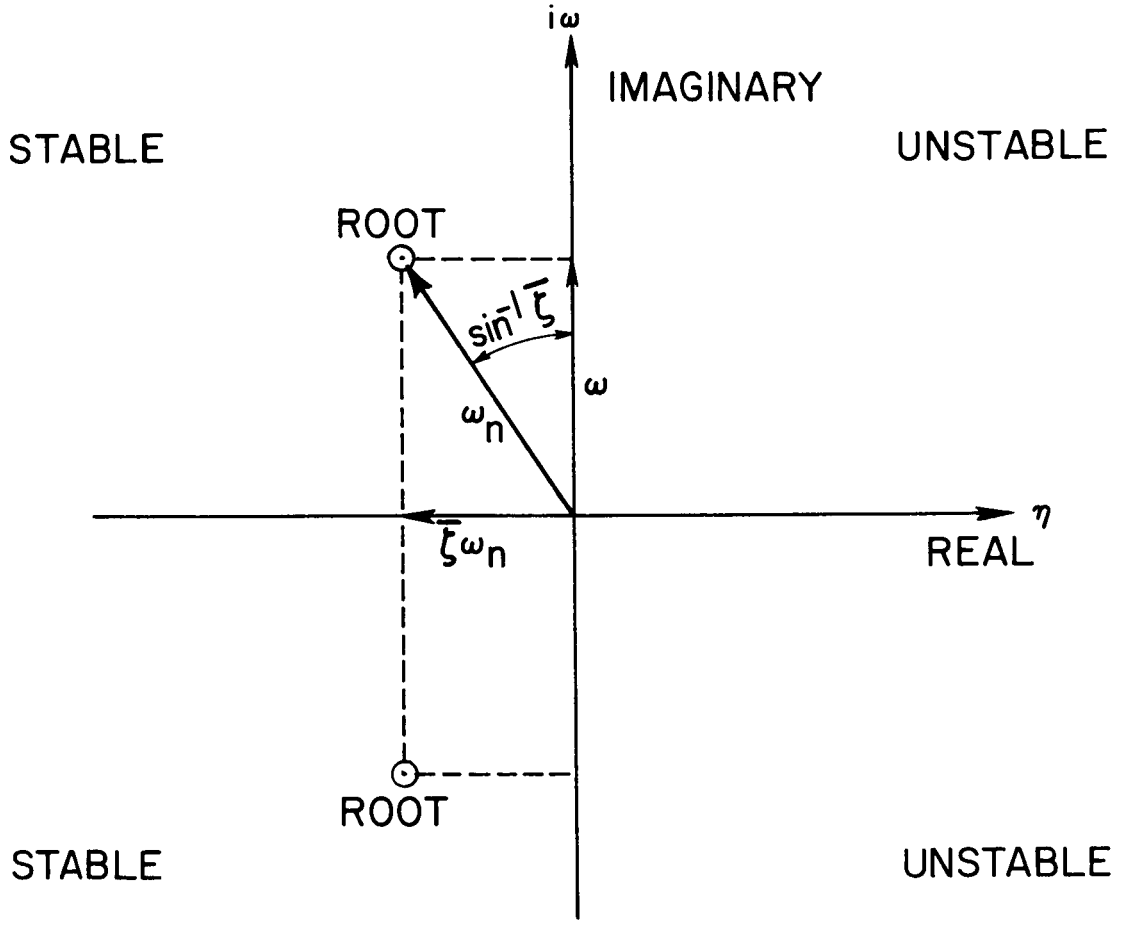

NASA

Figure 6.- Frequency and damping from root-locus plot.

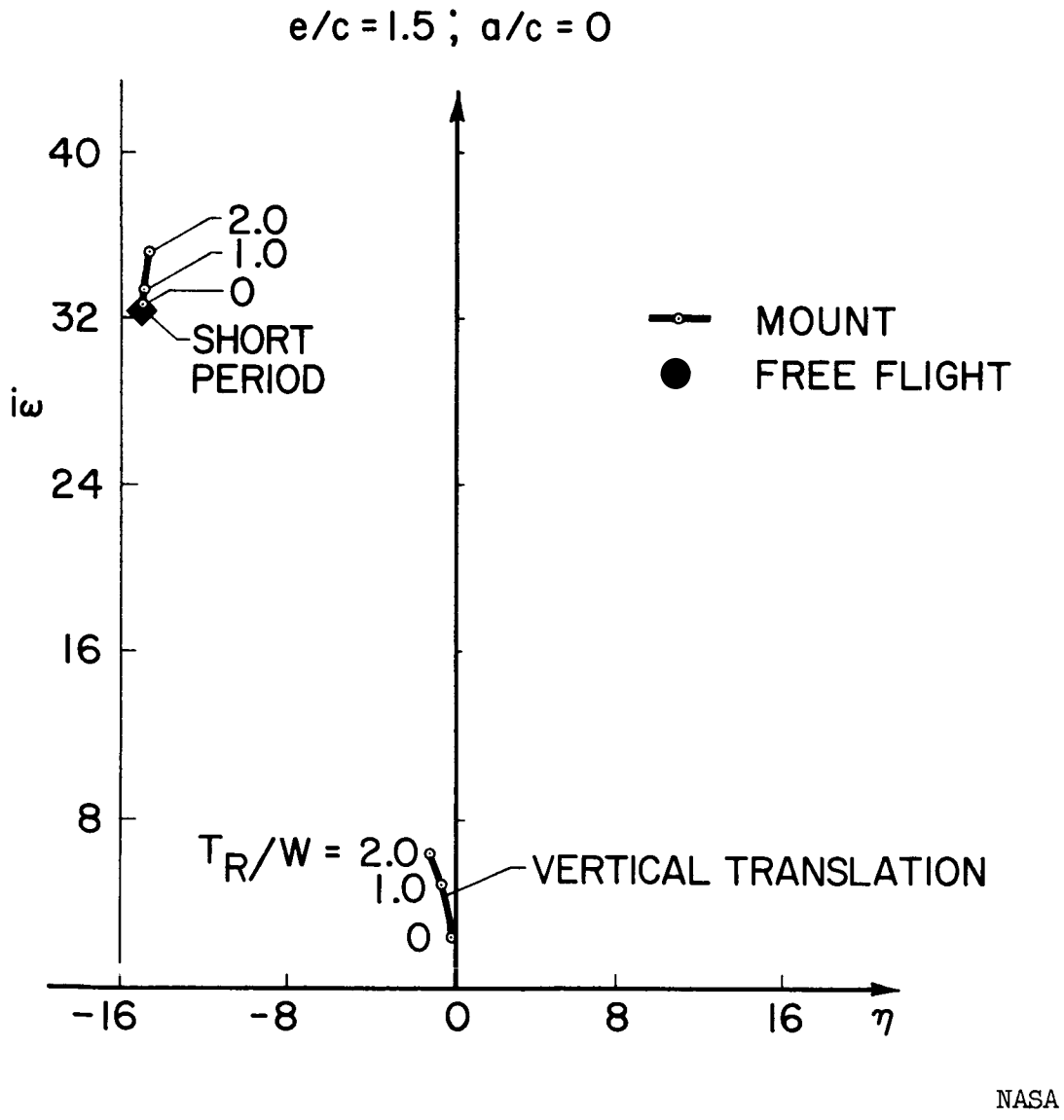

NASA

Figure 7.- Root locus of longitudinal modes.

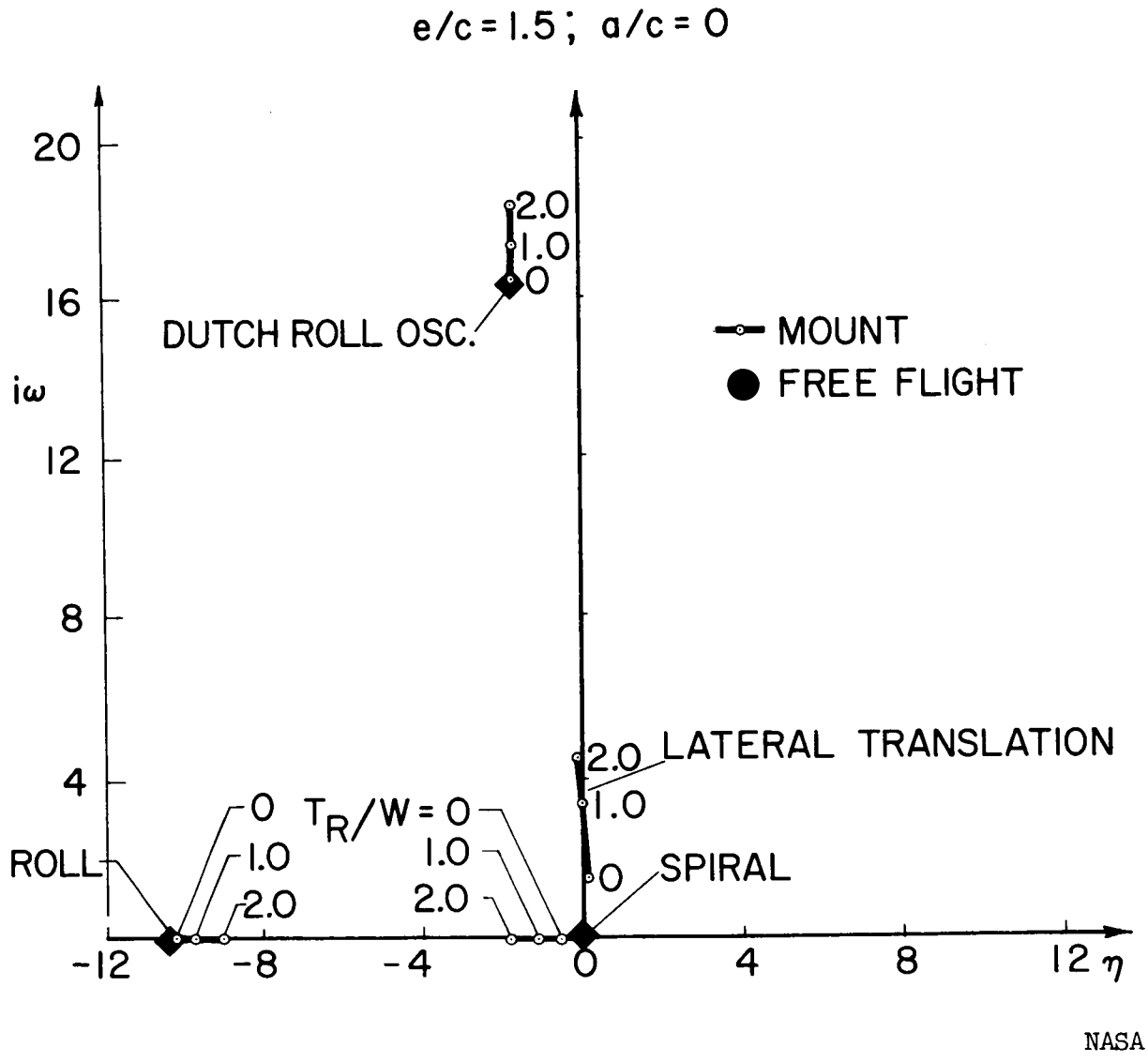

Figure 8.- Root locus of lateral modes.

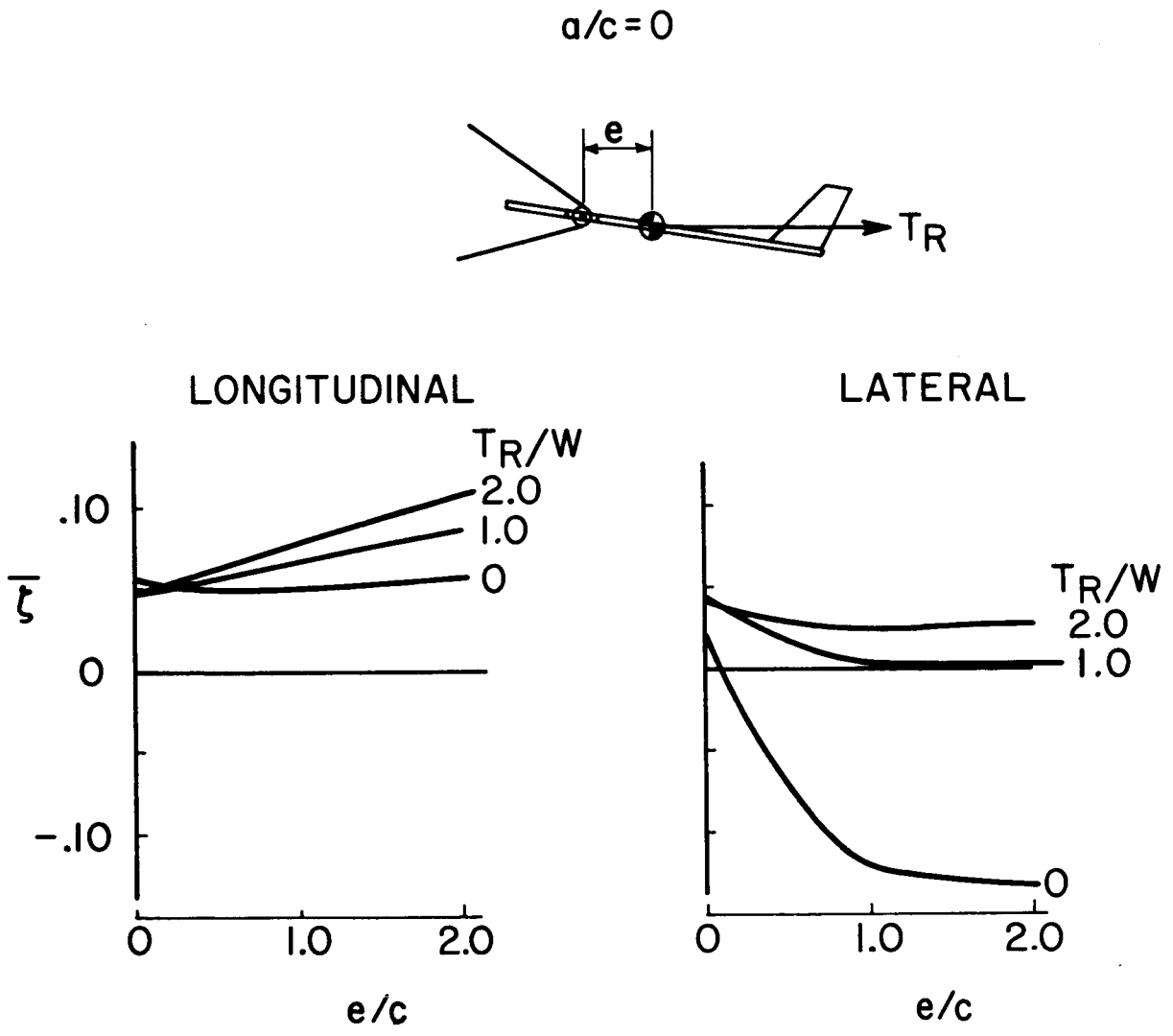

NASA

Figure 9.- Effect of front pulley location.

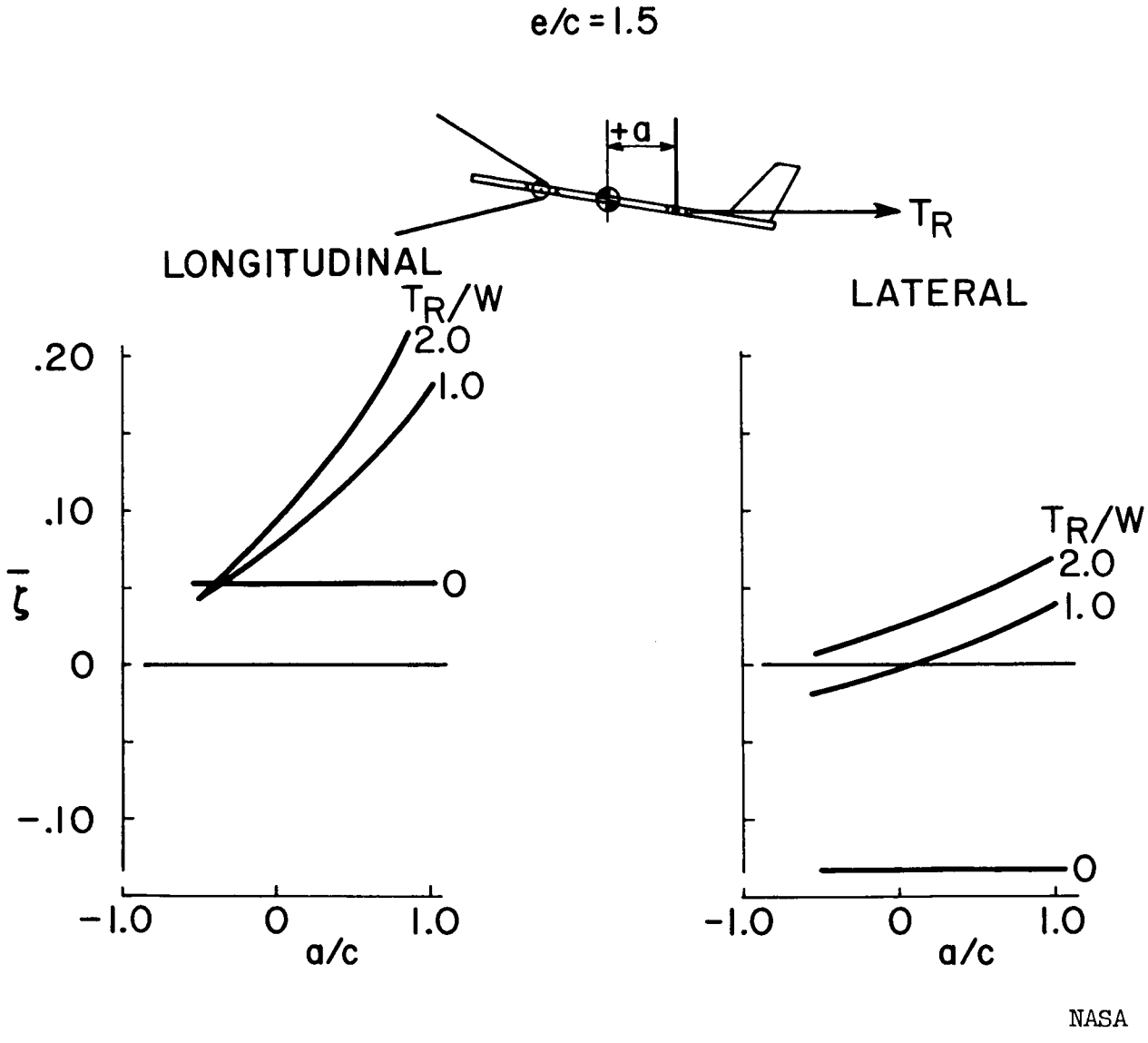

Figure 10.- Effect of rear pulley location.

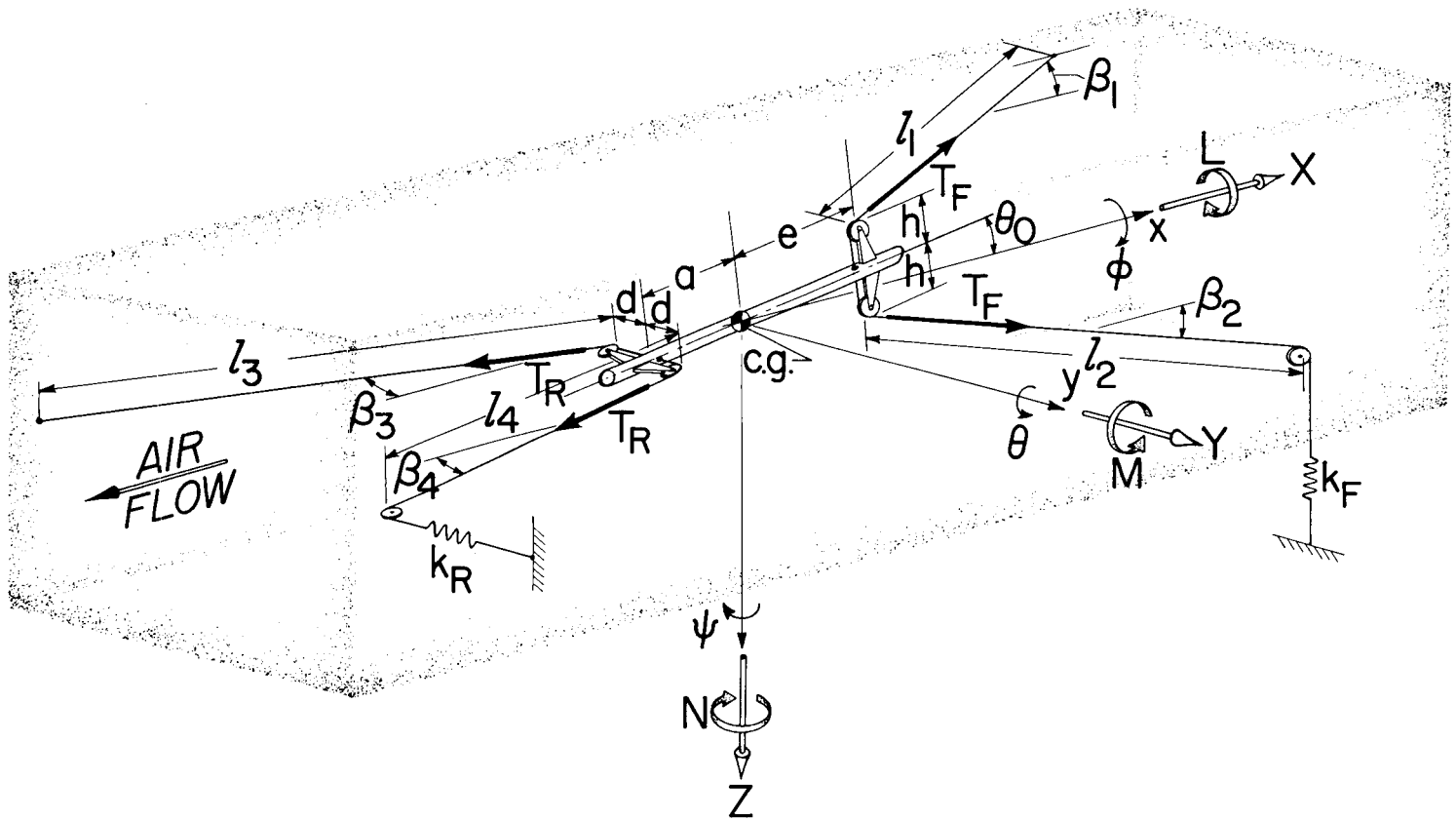

NASA

Figure 12.- Cable-mount configuration analyzed.

NASA-Langley, 1963

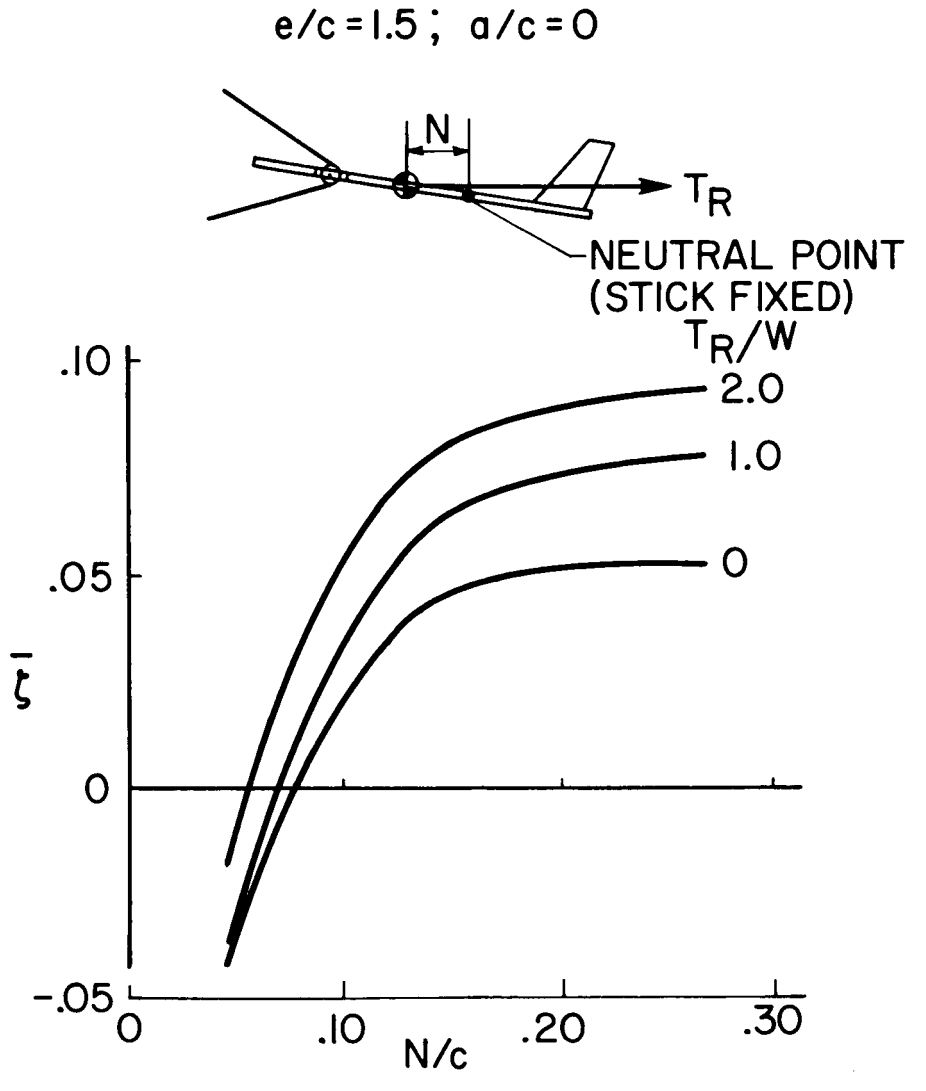

NASA

Figure 11.- Effect of static margin on longitudinal mode.